



1 **Canopy Area of Large Trees Explains Aboveground**
2 **Biomass Variations across Nine Neotropical Forest**
3 **Landscapes**

4
5
6

7 Victoria Meyer^{1,2}, Sassan Saatchi¹, David B. Clark³, Michael Keller^{4,5}, Grégoire Vincent⁶,
8 António Ferraz¹, Fernando Espírito-Santo^{1,7}, Marcus V.N. d'Oliveira⁵, Dahlia Kaki¹ and Jérôme
9 Chave²

10

11 ¹ *Jet Propulsion Laboratory, California Institute of Technology, Pasadena, CA, USA*

12 ² *Laboratoire Evolution et Diversité Biologique UMR 5174, CNRS Université Paul Sabatier, Toulouse,*
13 *France*

14 ³ *Department of Biology, University of Missouri, St. Louis, Missouri, U.S.A.*

15 ⁴ *USDA Forest Service, International Institute of Tropical Forestry, San Juan, Puerto Rico*

16 ⁵ *EMBRAPA Acre, Rio Branco, Brazil*

17 ⁶ *IRD, UMR AMAP, Montpellier, 34000 France*

18 ⁷ *Lancaster Environmental Centre, Lancaster University, Lancaster, United Kingdom, LA1 4YQ*

19

20

21

22 *Correspondence to:*

23 Victoria Meyer

24 *Jet Propulsion Laboratory*

25 *California Institute of Technology*

26 *4800 Oak Grove Drive*

27 *Pasadena, CA. 91109 USA*

28 *Email: victoria.meyer@jpl.nasa.com*

29

30

31

32

33

34

35



36 **Abstract**

37 Large tropical trees store significant amounts of carbon in woody components and their
38 distribution plays an important role in forest carbon stocks and dynamics. Here, we explore the
39 properties of a new Lidar derived index, large tree canopy area (LCA) defined as the area
40 occupied by canopy above a reference height. We hypothesize that this simple measure of forest
41 structure representing the crown area of large canopy trees could consistently explain the
42 landscape variations of forest volume and aboveground biomass (AGB) across a range of climate
43 and edaphic conditions. To test this hypothesis, we assembled a unique dataset of high-resolution
44 airborne Light Detection and Ranging (Lidar) and ground inventory data in nine undisturbed old
45 growth Neotropical forests. We found that the LCA for trees greater than 27 m (~25–30 m) in
46 height and at least 100 m² crown size in a unit area (1 ha), explains more than 75 % of total
47 forest volume variations, irrespective of the forest biogeographic conditions. When weighted by
48 average wood density of the stand, LCA can be used as an unbiased estimator of AGB across all
49 sites ($R^2 = 0.78$, RMSE = 46.02 Mg ha⁻¹, bias = 0.76 Mg ha⁻¹). Unlike other Lidar derived
50 metrics with complex nonlinear relations to biomass, the relationship between LCA and AGB is
51 linear. A comparison with tree inventories across the study sites indicates that LCA correlates
52 best with the crown area (or basal area) of trees with diameter >50 cm. The spatial invariance of
53 the LCA–AGB relationship across the Neotropics suggests a remarkable regularity of forest
54 structure across the landscape and a new technique for systematic monitoring of large trees for
55 their contribution to AGB and changes associated with selective logging, tree mortality, and
56 other types of forest disturbance and dynamics.

57 **Keywords**

58 Lidar, biomass, tropical forest, large trees, crown area, wood density



59 1 Introduction

60 In humid tropical forests, tree canopies contribute disproportionately to the exchange of water
61 and carbon with the atmosphere through photosynthesis (Goldstein et al., 1998; Santiago et al.,
62 2004). From a physical standpoint, canopies are rough interfaces formed by crowns of emergent
63 and large trees, regularly disturbed by wind thrusts and gap dynamics. This structurally complex
64 boundary layer is challenging for scaling of biogeochemical fluxes and modeling of vegetation
65 dynamics (Baldocchi et al., 2003). Large canopy trees are among the first to be impacted by
66 storms or heavy precipitation (Espírito-Santo et al., 2010), drought stress (Nepstad et al., 2007;
67 Saatchi et al., 2013; Phillips et al., 2009), and fragmentation (Laurance et al., 2000), potentially
68 leading to tree death and formation of large canopy gaps (Denslow, 1980; Espírito-Santo et al.,
69 2014). Several studies suggest that forest canopies can show fractal properties that tend to evolve
70 from a non-equilibrium state towards a self-organized critical state, involving gap formation and
71 recovery (Pascual and Guichard, 2005; Solé and Manrubia, 1995), with crowns preferentially
72 growing towards more sunlit parts of the canopy (Strigul et al., 2008).

73 Over the past decade, stand level canopy metrics have been increasingly derived using small
74 footprint airborne Lidar systems (ALS), a widely used remote sensing technique to study the
75 structure of forests (Kellner and Asner, 2009; Lefsky et al., 2002). Lidar derived mean canopy
76 height (MCH) is a good predictor of tropical forest aboveground carbon content and its spatial
77 variability (Jubanski et al., 2013), but it does not provide information on the presence of large
78 trees that are important when monitoring changes of forest biomass from logging and small scale
79 disturbance (Bastin et al., 2015). Moreover, different forests with the same MCH may differ in
80 their stem density, notably of large trees, and in stand mean wood density, two aspects that are
81 important in constructing a robust model to infer AGB from lidar data (Asner et al., 2012;



82 Mascaro et al., 2011). Ground observations suggest that stem density, basal area, height and
83 crown size of large tropical trees may all be good indicators of forest AGB (Clark and Clark,
84 1996; Goodman et al., 2014). This implies that including information on crown area of
85 individual large trees should improve carbon stock assessments, as confirmed in temperate and
86 boreal regions (eg. Packalen et al., 2015; Popescu et al., 2003; Vauhkonen et al., 2011, 2014). In
87 tropical forests, identifying and delineating crowns of large trees is a difficult and time
88 consuming process due to the layered structure of the forest canopy and overlapping crowns
89 (Zhou et al., 2010, but see Ferraz et al., 2016).

90 Here, we explore how the fractional area occupied by crowns of large trees in a forest stand can
91 be used as a reliable indicator of forest biomass across a wide range of forest structure, climate
92 and edaphic geographic variations. We define large tree canopy area (LCA) as a metric
93 capturing the cluster of crowns of large trees within a forest patch using height and crown area
94 measured by high resolution airborne Lidar measurements. Precisely, LCA is the number of
95 pixels in the canopy height model above a reference height, and excluding the pixel clusters
96 smaller than a reference area. Since this metric quantifies the proportional presence of large
97 trees, it can be used to estimate AGB and monitor changes associated with the disturbance of
98 large trees from mortality events and selective logging. We first explore the properties of LCA
99 across a range of landscapes in the Neotropics. Next, we hypothesize that LCA is a good
100 predictive metric of the spatial variations of AGB over a wide range of old growth forests.

101 To this end, we assembled a collection of airborne Lidar measurements and ground inventory
102 data at nine sites in old growth Neotropical forests. The Lidar data provide variations in canopy
103 height and distribution of large trees that allow us to address the following questions: 1) is there



104 a unique definition of LCA at the landscape scale across different sites? 2) does LCA metric
105 capture variations of AGB?

106

107 **2 Materials and Methods**

108 **2.1 Study sites**

109 We studied the canopy structure at nine old growth lowland Neotropical forest sites that span a
110 broad range of climatic and edaphic conditions (Fig. S1, Table 1). All sites are located in low
111 elevation areas (less than 500 m above sea level) but have small scale surface topography that
112 may influence the distribution of crown formations and gaps. These forests are for the most part
113 undisturbed *terra firme* forests. Tapajós, Antimary and Cotriguaçu get the least rainfall, with
114 approximately 2000mm yr⁻¹, while La Selva and Chocó both receive more than 4000 mm yr⁻¹
115 (Table 1).

116 Permanent forest inventory plots were available for all sites except Cotriguaçu (Table 1). Sites
117 where tree level inventory data were available were used to estimate the stand level aboveground
118 biomass, thereafter referred to as AGB_{inv}. BCI (50 plots of 1 ha each), Chocó (42 plots of 0.25 ha
119 each), La Selva (11 plots of 1 ha each), Manaus (10 plots of 0.25 ha each), Nouragues (7 plots of
120 1 ha each) and Tapajós (10 plots of 0.25 ha each). In these plots, all trees with a diameter at
121 breast height (DBH) ≥10 cm have been mapped, measured and identified to the species. Trees
122 with irregularities or buttresses were measured higher on the bole. Total tree height
123 measurements were available for a subset of these trees. The method for calculating AGB_{inv} from
124 forest inventories at 1 ha scale is reported in S.1 of the supplementary information. Stand
125 averaged wood density of each site was calculated and is reported in Table 1. Additional plot



126 level data (AGB_{inv} and mean wood density) were provided for Antimary (50 plots of 0.25 ha
127 each), Nouragues (27 plots of 1 ha each) and Paracou (85 plots of 1 ha each).
128 The four sites where 1 ha plots were available were used to compare the LCA metric and AGB,
129 and are here referred to as “calibration sites” (BCI, La Selva, Nouragues and Paracou). Smaller
130 plots have a higher probability of having the crown of large trees extend outside the plot
131 boundary, which can introduce uncertainty in estimates of LCA because of edge effect (Meyer et
132 al., 2013; Packalen et al., 2015). For this reason, all plots smaller than 1 ha were excluded from
133 this analysis.

134

135 **2.2 Lidar data**

136 Lidar sensors scan the vegetation vertical structure and return a three dimensional point cloud
137 derived from the time it took each pulse to return to the instrument. The Lidar datasets acquired
138 over the study sites come from discrete return Lidar instruments and were gridded horizontally at
139 a 1m resolution using the echoes classified as either vegetation or ground. They yield three
140 products: digital surface model (DSM) corresponding to the top canopy elevation, digital terrain
141 model (DTM) corresponding to the ground elevation, and canopy height model (CHM), which is
142 the height difference between the DSM and the DTM. DTMs were interpolated from a Delaunay
143 triangulation or comparable interpolation methods, after outliers have been removed. DSMs were
144 created using the highest return within a cell. Lidar data over Paracou were acquired in last
145 return mode, causing a bias of 50 cm on the CHM (Vincent et al., 2012). This bias is not
146 addressed in this study because our height increment for the determination of optimal height
147 thresholding is larger (1m) (see Sect. 4.3). Data were acquired between 2009 and 2013, using



148 relatively similar sensors and acquisition configurations (Table 2). The potential differences
149 between the Lidar datasets and their impact on the results are addressed in the Discussion.
150 For each site, we selected a 1x1 km (100 ha) area of old growth forest, oriented north-south,
151 without any human disturbance to the extent possible. Topography derived from Lidar data
152 within the selected 1 km² subset images provides information on landscape variations that may
153 impact the forest structure. Data visualization was done using ENVI version 4.8 (Exelis).
154 Mean canopy height (MCH) is a good predictor of AGB provided that the regression model is
155 calibrated locally. It was calculated by averaging all the canopy height model pixels falling in an
156 area of interest. Here, we calculated an AGB map of each site from MCH using the following
157 model form (Eq. (1), Asner and Mascaro, 2014).

$$158 \quad AGB_{Lidar} = aMCH^b + \epsilon \quad (1)$$

159 where AGB_{Lidar} is the aboveground biomass estimation derived from Lidar data, a is a scaling
160 constant, which is expected to depend significantly on forest type and stand level wood density,
161 b is a power law exponent and $\epsilon \sim N(0, \sigma^2)$ represents the uncertainty in measurements. All
162 coefficients are presented in Table S1. We inferred the model parameters directly for the sites
163 where AGB_{inv} of 1 ha plots was available (La Selva, BCI, Paracou and Nouragues). For Chocó
164 and Antimary, we developed models based on 0.25 ha plots and 50 m x 50 m pixels of Lidar data
165 and after estimating AGB_{Lidar} , aggregated the image to 1 ha or 100 m pixels. For the remaining
166 sites of the Central Amazon (Cotriguaçu, Manaus and Tapajós), we used a model based on
167 existing data derived from airborne and spaceborne Lidar (Lefsky et al., 2007). This model may
168 have larger uncertainty in estimating biomass compared to our site specific model, but we here
169 assume that all 1 ha scale AGB_{Lidar} estimates have approximately similar uncertainties.

170



171 **2.3 Computing Large Canopy Area (LCA)**

172 At each study site, we extracted the area of canopy that relates to total area of the canopy height
173 model above a standard height (h) threshold, or LCA(h), and explored how this metric scales
174 along two axes. First, we varied the threshold height h with increments of 1m, between 5m and
175 50m, in 100 m by 100 m subareas (100 subareas for each site). Second, to denoise the data, we
176 excluded the clusters with less than a set number of 1m² pixels (50, 100, 150 or 200). We then
177 prioritized the crown area of large trees, and filtered out pixels that could be related to outliers or
178 to single branches. This method thus quantifies the area of large crowns covering a plot or larger
179 landscape unit area, as a percentage of covered area.

180 LCA maps were produced at 1 ha resolution. Pixel clustering was based on the similarity of the
181 four nearest neighbors (similar results were obtained with an eight neighbor model, results not
182 shown here). Figure S2 summarizes the steps taken to go from the Lidar canopy height model to
183 the final LCA map. Processing was conducted using the IDL software (Interface Description
184 Language, Exelis).

185 We determined the optimal minimum crown size and canopy height threshold calculating the
186 coefficient of correlation between AGB_{Lidar} and LCA. We also performed the same analysis
187 using AGB_{inv} and LCA at the four calibration sites. This step allowed us to examine if optimal
188 height thresholds differed from one site to the other. The goal was to find a single optimal height
189 threshold and crown size that could be applied for LCA retrieval across closed canopy
190 Neotropical forests.

191

192 **2.4 Relating LCA to biomass**



193 We tested different models to infer AGB_{inv} from LCA, henceforth called AGB_{LCA} , at the four
194 calibration sites, and explored if adding more parameters, such as mean wood density of a site,
195 mean wood density of large trees ($DBH \geq 50$ cm), mean canopy height or top percentiles of
196 canopy height improved the predicting power of the model. The two models we retained are of
197 the form of Eq. (2) and Eq. (3):

$$198 \quad AGB_{LCA} = a LCA + b \quad (2)$$

$$199 \quad AGB_{LCA} = (a LCA + b) \times WD \quad (3)$$

200 where WD is the mean wood density of a site or the mean wood density of trees >50 cm in DBH
201 of a site.

202 We evaluated our results by applying a jackknife validation to our regression model, based on
203 1000 iterations of bootstrapping. We also compared AGB as derived from LCA (AGB_{LCA}) to the
204 Lidar derived aboveground biomass (AGB_{Lidar}) in the nine 1km^2 images. Coefficients of
205 correlation (R^2), root mean square error (RMSE) and bias are reported. We finally compared
206 these results to a traditional model relying on MCH to estimate AGB. The analysis was
207 performed using the R statistical software (R Core Team, 2014).

208

209 **2.5 Detecting Changes of Selectively Logging**

210 Forest degradation due to selective logging is difficult to detect with conventional remote
211 sensing techniques due to small scale and minor impacts on the forest canopy and biomass
212 compared to severe forest disturbances (e.g. fires, storms, or clearing). However, selective
213 logging targets large trees (Pearson et al., 2014) and thus may be detectable using LCA. Here, we
214 use the Antimary study site that was selectively logged after the 2010 Lidar acquisition to
215 examine the use of LCA for detecting logging impacts on the forest canopy and AGB. We apply



216 the large tree segmentation approach on both the 2010 and on a 2011 post-logging Lidar data
217 (see Andersen et al., 2014 for details) to quantify the logging impacts in terms of the distribution
218 of large trees removed from the forest and the loss of aboveground biomass.

219

220 **3 Results**

221 **3.1 Intersite comparison of landscapes and MCH**

222 Topographic variation ranged from about 4 m elevation gain in flat area of Tapajós to steep
223 elevation gain of up to about 100 m in Cotriguaçu and Chocó (Fig. S3). Top canopy height
224 reached up to 60m, but varies across sites, with Chocó having the lowest MCH (24.1 m) and
225 Nouragues the highest (29.7 m). Forest height in Manaus was more homogeneous than in the
226 other sites, with a standard deviation of 6.8 m for MCH, versus 10.3 m in Paracou. We found no
227 relationship between topography and canopy height, which suggests that variability in forest
228 structure may be due to other ecological and edaphic factors in each site.

229

230

231 **3.2 Large canopy area index**

232 The choice of the canopy height threshold impacted LCA more than the minimum number of
233 pixels per cluster (Table S2). The difference due to the choice of the minimal cluster size
234 threshold was on average 1.4 %, calculated as the mean of the difference between the smallest
235 grain (50 pixels) and the largest one (200 pixels) across sites and height thresholds. Based on this
236 analysis, we chose to define LCA using a minimum cluster size of 100 pixels (100 m² for crown
237 area) in the remainder of this study. This corresponds to an area of at least 10 m x 10 m or a circle
238 of approximately 11m in diameter, consistent with the average crown diameter of large trees of
239 the region (Bohlman and O'Brien, 2006; Figueiredo et al., 2016; Clark, unpublished results).



240
241 In contrast, the canopy height thresholds markedly impacted the magnitude of LCA among sites
242 (Fig. 1 and Fig. 2, Table S2). As the height threshold increased, intra-site variation of LCA(h)
243 became apparent, showing differences of LCA associated with differences of forest structure
244 (Fig. 1). Tapajós and Nouragues stood out with more area of large trees at the height threshold of
245 30 m ($LCA_{30m} = 51$ and 48 %, respectively) , while Antimary and Chocó showed much lower
246 LCA at this height threshold ($LCA_{30m} = 21$ %) (Table S2). The steepest slopes of the LCA(h)
247 function corresponded to the highest sensitivity of LCA to height thresholds and the inflection in
248 LCA was found between 24m in Antimary and 30m in Nouragues (Fig. 2). The average height
249 of the steepest slope was about 27 m, a value that was used as the optimal threshold across all
250 sites.

251 Regressing AGB_{Lidar} and LCA showed that the highest coefficients of correlation between the
252 two metrics occurred between 23 m (Chocó) and 30 m (Tapajós) height thresholds (Fig. 3a),
253 explaining more than 75 % of AGB variation in each site. The same analysis repeated using
254 AGB_{inv} and LCA at the calibration sites (Fig. 3b) also confirmed the earlier results showing the
255 best relationships corresponded to height thresholds are found to be between 27m (Nouragues
256 and Paracou) and 28m (BCI and La Selva), with maximum coefficients of correlation ranging
257 between 0.5 and 0.8. Based on these results, we defined LCA as the cumulative area of clusters
258 of the canopy height model greater than 27 m height and each more than 100 m^2 .

259

260 3.3 Variation of AGB derived from LCA

261 AGB_{inv} was found to depend linearly on LCA (Eq. 2), with a better coefficient of correlation and
262 RMSE than other models, such as a power law fit ($R^2_{linear} = 0.59$, $RMSE_{linear} = 62.53 \text{ Mg ha}^{-1}$, vs.
263 $R^2_{power} = 0.54$, $RMSE_{power} = 65.38$). Although this model was unbiased ($bias = 0.0 \text{ Mg}$, $bias_{cross_val}$



264 = 0.16 Mg), there were clear differences among study sites (Fig. 4, Table 3). These differences
265 were largely explained by landscape scale differences in wood density, an important factor
266 representing the influence of species composition on the spatial variation of AGB. To explore the
267 contribution of wood density across the study sites, we computed the average wood volume as
268 the ratio of AGB divided by the average wood density (Fig. 4b). The linear relationship
269 between LCA and wood volume yielded an estimate of the average total volume of forests
270 independently of the site characteristics, through $\text{Vol} = a \text{LCA} + b$ (Table 3).

271 For AGB estimation, the model based on LCA weighted by WD gives the best result by bringing
272 R^2 up to 0.78 and RMSE down to 46.02 Mg ha⁻¹ (Fig. 4b, Fig. 5, Table 3, Eq. (3)), with AGB_{inv}
273 and AGB_{LCA} falling around a one-to-one line in Fig. 5a. At all sites, RMSE values are between
274 20.87 and 42.22 Mg, except Nouragues, where RMSE remains large (71.21 Mg) due to high
275 biomass and several outliers from the linear relation.

276 Finally, we applied the model from Eq. (3) to all 1km² areas and compared the derived AGB_{LCA}
277 to $\text{AGB}_{\text{Lidar}}$ (see Sect. 2.2), for which local models based on MCH were used (Fig. 5b). Global
278 RMSE was found to be 34.72 Mg and RMSE per site varied between 20.79 Mg at BCI and 49.58
279 Mg at Manaus. Our ground calibrated LCA model defined by Eq. (3) had a similar performance
280 as the MCH based AGB model ($R^2_{\text{MCH}} = 0.79$, $\text{RMSE}_{\text{MCH}} = 44.2$ Mg, Table S3). These findings
281 show that relying on a fraction of the Lidar information gives comparable results as using
282 metrics depending on information from all pixels, such as MCH, highlighting the importance of
283 large canopy trees to estimate biomass. The relationship between LCA and other metrics derived
284 from ground data, such as Lorey's height or basal area, are presented in Table S4.

285

286 3.4 AGB changes from logging



287 The impacts of logging on the distribution of large trees and changes of AGB was detected by
288 simply deriving the LCA index from pre and post-logging Lidar data acquired in 2010 and 2011
289 respectively in Antimary (Fig. 6). Difference in LCA between the two dates (2010–2011) (Fig.
290 6a) at 1 ha grid cell captured the areas of largest changes in the few months following logging
291 (logging took place between June and November 2011, Lidar data were collected in late
292 November 2011). The LCA approach was able to detect approximately a 17 % decrease in LCA,
293 from a mean LCA of 34.8 % in 2010 to 29.2 % in 2011.

294 The changes were also captured in the frequency distribution of large canopy trees before and
295 after logging (Fig. 6b) and the differences in the spatial distribution (Fig. 6c and 6d).

296 These changes in LCA correspond to a biomass loss of 15.2 Mg ha⁻¹ when integrated in equation
297 (2) and were of the same magnitude of the planned selectively logging removal rate (12–18 Mg
298 ha⁻¹ or 10–15 m³ ha⁻¹ of timber volume) (Andersen et al., 2014). Difference in the Lidar index
299 (ΔLCA) at the native resolution of 1 m (Fig. 6e) was able to capture both the location of all large
300 trees removed from the forest stand and partial regeneration and gap filling that occurred in the
301 forest between the two dates.

302

303 **4 Discussion**

304 **4.1 Inter-site Comparisons**

305 Cross-site studies on the structure of tropical forests have led to significant advances in our
306 understanding of tropical forest ecology (Gentry 1993; Phillips et al., 1998; ter Steege et al.,
307 2006). They have also yielded important insights on new techniques to predict carbon stocks
308 across regions (eg. Asner and Mascaro, 2014). Comparison of sites in terms of MCH derived
309 for the study sites confirms that there is a strong regional variations of AGB with respect to



310 canopy height, and that East Amazonian sites tend to have much taller trees than Central and
311 Western Amazonia sites. This was already apparent in the canopy height maps produced by the
312 GLAS sensor (Lefsky, 2010; Saatchi et al., 2011; Simard et al., 2011). Comparing sites in terms
313 of LCA showed a similar pattern of larger trees, being relatively more present in eastern
314 Amazonia, notably in the French Guiana sites and Tapajos. Our most southwestern site was
315 Antimary, in the state of Acre (Brazilian Amazon) and does not represent areas in the Peruvian
316 Amazon and western Amazon-Andes gradients. The site in Chocó is also unique in its
317 characteristics because of extremely wet condition and unknown disturbance history (e.g.,
318 selective logging). Additional lidar and ground measurements would be needed in western
319 Amazonia to further validate the patterns observed in this study.

320

321 **4.2 Physical Interpretation of LCA**

322 In this study, we introduced a simple structural metric that captures the proportion of area
323 covered by large trees over the landscape (> 1 ha) and explained the variation in average forest
324 volume and biomass when weighted by wood density in nine sites of old growth Neotropical
325 forests. LCA cannot separate the crown areas of individual trees. However, it is adapted for
326 large scale monitoring of forest volume and biomass change, as it is a robust and readily
327 accessible metric. For individual tree separation, complex and more computationally intensive
328 approaches are available (Ferraz et al., 2016).

329 In estimating LCA from Lidar data, we examined the spatial clustering properties of LCA and
330 found that the minimum cluster size was less important than the threshold of canopy height, as
331 long as the analysis focused on the relative covered area instead of on the density of large trees.
332 We found that using the percentage of the area covered by large canopy trees is an efficient way



333 of overcoming the problem of individual crown segmentation in Lidar data. LCA is related to
334 how trees reaching the forest canopy (above a certain height) fill the space and how this
335 characteristic may follow a spatially invariant scaling across tropical forests (West et al., 2009).

336

337 **4.3 Correlation between LCA and AGB**

338 The distribution of R^2 between LCA and AGB for (Fig. 3) is such that the maximum difference
339 in R^2 between a threshold of 25m and 30m is approximately 0.1, a negligible value. Hence, AGB
340 retrieval by LCA is relatively insensitive to the height threshold. For most sites, except

341 Antimary, we found a height threshold such that LCA explains about 80–90 % of the variation of
342 AGB or total volume of the forests for each site (60–70 % when compared with ground plots).

343 Using a height threshold of 27 m for all sites reduced the R^2 by 0.04 on average (max = 0.08)
344 compared to the optimal height threshold for each site. Hence, the difference between the R^2 of

345 Lidar and ground plots is due to the relative correlation between MCH used in Lidar derived
346 biomass and LCA. Differences in Lidar characteristics for each site and differences in timing of
347 Lidar observations and ground plots further amplify this problem. Finally, a limit to how much
348 LCA can explain variation in AGB relates to forest structure and the AGB of small trees.

349 Potential differences in MCH among sites are due to footprint size, scan angle and return density
350 (Disney et al., 2010; Hirata, 2004; Hopkinson, 2007). However, these effects are generally
351 smaller than the 1m increment that we used to determine the optimal height thresholds of LCA.

352 As a result, LCA estimation, and therefore AGB inferred from LCA, should depend little on
353 instrument, acquisition and processing (Table 2). This is an important finding given the
354 increasing variety of airborne Lidar sensors, and also given the pre and post-processing methods
355 available for monitoring tropical forest structure and aboveground biomass. However,



356 determining whether the 27m threshold holds for LCA calculation across in the tropics would
357 require a validation at more study studies across continents.

358

359 **4.4 LCA Relation to Ground Measurements**

360 The relation between LCA derived from Lidar and the ground measurements can be investigated
361 by converting the 27 m height threshold into equivalent DBH values, using a height–diameter
362 relationship. In the absence of a local DBH–height relation at each site, we made use of the
363 following equation (Chave et al., 2014):

$$364 \quad \ln(H) = 0.893 - E + 0.760 \times \ln(D) - 0.0340 \times (\ln(D))^2 \quad (4)$$

365 where E is a measure of environmental stress for each site that potentially impacts the tree
366 allometry. The corresponding DBH values fall around 35–55 cm, except for Chocó, where the
367 best coefficient of correlation is reached with a DBH threshold of 29 cm (Fig. S4). The DBH
368 estimation suggests that using a minimal DBH threshold of about 50 cm for large trees for old
369 growth neo-tropical forests better represents the total AGB variations.

370 The lower range of biomass estimation for the LCA model, associated with the intercept for LCA
371 equal to zero, ranged between 122 Mg ha⁻¹ in La Selva and 192 Mg ha⁻¹ in Paracou (Fig. 7a).

372 This lower range identified with the intercept of the LCA–AGB linear model can be interpreted
373 as the AGB associated with all trees smaller than 27 m and representing the smaller trees
374 (approximately all trees with DBH <50 cm). Note that the differences between sites are only due
375 to differences in their mean wood density and not the volume of trees (see Eq.(3) and Fig. 4).

376 Similarly, the contribution of small trees to the total biomass in the ground inventory ranges

377 between around 100 and 200 Mg ha⁻¹, except in Paracou (261 Mg ha⁻¹) (Fig. 7b). AGB

378 estimation based on LCA in these sites cannot go under 100 Mg ha⁻¹ or over 500 Mg ha⁻¹. This



379 is not a limitation of the model because LCA is designed to provide AGB estimates for forests
380 reaching at least 27 m in mean canopy height, and such forests generally exceed 100 Mg ha⁻¹ in
381 AGB. Also, the upper threshold of 500 Mg ha⁻¹ is consistent with upper values found globally at
382 1 ha scale (Brienen et al., 2015; Slik et al., 2013). A recalibration of the method should be
383 envisaged in secondary and highly degraded forests.

384

385 **4.5 LCA as AGB Estimator**

386 The correlation of LCA to AGB_{inv} suggests that a Lidar based approach can lead to the
387 estimation of AGB at the landscape scale and give useful information on the presence of large
388 canopy trees and their distribution, extending the analysis of large trees in plot level inventory
389 based studies (Bastin et al., 2015; Slik et al., 2013).

390 Therefore, LCA can explain the variations of total forest volume without any ancillary data
391 about the forest or the landscape. Any bias in conversion of LCA to AGB, however, can be
392 corrected across landscapes and sites by scaling the LCA–AGB relationship with average wood
393 density at the landscape scale.

394 Wood density has been shown to be a key element of allometric models of AGB estimation
395 (Baker et al., 2004; Brown et al., 1989; Chave et al., 2004; Nogueira et al., 2007). If wood
396 density is assumed to be constant across DBH classes, the mean wood density at the plot scale
397 can readily be used to scale LCA to biomass. However, if the wood density of large trees is
398 smaller or larger than the average wood density, (e.g. in BCI and Chocó: S.3, Fig. S5), the use of
399 mean wood density to scale LCA may introduce a slight bias in biomass estimation. A difference
400 in mean wood density of 0.1 g cm⁻³ would introduce a bias of ±10 % in the biomass estimation
401 when using our model. We found that using mean wood density of large trees or basal area



402 weighted wood density instead can give slightly better results and could circumvent the
403 differences in size distribution of the wood density (S.3). Instead we could rely on the wood
404 density of large trees only. This would make the collection of ground data easier and cost
405 effective for biomass estimation, because trees ≥ 50 cm DBH only represent 5–10 % of the stems
406 of a plot (S.3, Fig. S6). Focusing on the wood density of dominant or hyper dominant species
407 could also be an alternative approach for future use of Lidar derived LCA for large scale biomass
408 estimation (Fauset et al., 2015; ter Steege et al., 2013).

409

410 Both MCH and LCA–AGB models performed relatively poorly in high biomass plots of the
411 Nouragues study area, by underestimating biomass values >500 Mg ha⁻¹ (Fig. 4 and 5). To
412 explain the underestimation, we performed three tests: 1. We examined the differences in the
413 ground estimated biomass values with and without tree height and found no significant impact in
414 reducing the effect of underestimation. 2. We tested the hypothesis that the height threshold
415 used for LCA estimation across sites was not suitable for the Nouragues study site and dismissed
416 the hypothesis because 27 m was found to be the optimum threshold for Nouragues plots. 3. We
417 examined the errors in the Lidar estimation of forest height and found that except for an
418 extremely high AGB_{inv} of 617 Mg ha⁻¹, the four other high biomass outliers are all located in the
419 6 ha Pararé plot located on a very steep topography. The Lidar digital terrain model (DTM) of
420 this area shows an average within plots elevation range of 90 m. Ground detection on steep
421 terrain can be erroneous, depending on the Lidar point density and the view angle, causing large
422 area interpolation errors for DTM development and significant error in canopy height
423 measurements (Leitold et al., 2015). Other factors that may affect the underestimation of AGB



424 by LCA or MCH in the Nouragues site may be due to the presence of forest patches with clusters
425 of large trees and overlapping crown areas.

426

427 **4.6 LCA and forest degradation**

428 Although LCA and MCH may perform similarly in capturing the forest biomass variations and
429 changes, the use of LCA in detecting forest degradation and logging is more straightforward
430 because of its relation to large trees. The LCA approach was able to accurately detect changes
431 in forests after logging by locating where the large trees are extracted. Our estimate of biomass
432 change from the LCA approach was higher than the biomass loss of 9.1 Mg ha^{-1} reported by
433 another study using the 25th percentile height above ground as the Lidar metric for biomass
434 estimation (Andersen et al. 2014). It can be expected that relying on the 25th percentile height
435 metric for biomass estimation would place more emphasis on the lower part of the canopy
436 (understory) that is either less damaged or has gone through some level of regeneration after
437 logging. Models based on LCA or MCH, on the other hand, may be more realistic for estimating
438 AGB changes because they capture the changes in large trees and upper forest canopy structure
439 that contain most of the biomass and are directly impacted by logging and biomass removal.

440

441 **4.7 Future Applications of LCA**

442 LCA definition in our study relies on the high resolution information on forest height, allowing
443 for the detection of crown area of large canopy trees. Can a similar measure be derived from
444 large footprint Lidar observations such as the future NASA spaceborne Lidar mission GEDI
445 (Global Ecosystem Dynamic Investigation)? GEDI will not provide spatially continuous data



446 on forest height, but its footprint size (~ 25 m) and dense sampling may be adequate to develop
447 statistical indicators of large trees over the landscape.

448 Similarly, future spaceborne radar missions could also provide useful information to retrieve
449 large canopy areas. The synthetic aperture radar (SAR) tomographical observations of the
450 European Space Agency (ESA) BIOMASS mission will provide wall-to-wall imagery of canopy
451 profile that could be converted to LCA over the landscape (Le Toan et al., 2011). Preliminary
452 research based on airborne TomoSAR measurements has already shown that backscatter power
453 at about 30 m above the ground, with sensitivity to the distribution of large trees, explained the
454 variation of AGB over Nouragues and Paracou plots better than the backscatter power related to
455 the lower part of the canopy (0–15 m) (Minh et al., 2016; Rocca et al., 2014). Future research on
456 exploring the use of an equivalent radar index product from BIOMASS height or tomography
457 measurements at a height threshold (e.g. 27 m) may provide a potential algorithm to map the area
458 of large trees and estimate forest volume and biomass changes across the landscape.

459

460 **5 Conclusions**

461 We introduce LCA as a new Lidar derived index to capture the variations of large trees and total
462 volume and biomass across landscapes that remain spatially and regionally invariant. The
463 importance of LCA is in its relevance to the structure and ecological characteristics of large trees
464 in filling the canopy space and their unique contribution in determining the total volume and
465 biomass of forests. Unlike other Lidar derived metrics, LCA is linearly related to total
466 aboveground biomass after being weighted by average wood density and this linear relationship
467 remains unique across different forest types. The comparison of LCA index with ground plots
468 suggests that DBH >50 cm is a more reliable threshold to quantify the number and distribution of



469 large trees and in capturing the variations of the total aboveground biomass across landscapes
470 and regions.

471

472 **Author contribution**

473 V. Meyer and S. Saatchi developed the model and designed the study. V. Meyer developed the
474 model code and performed the analysis. J. Chave, G. Vincent, M. Keller, F. Espírito-Santo, D.
475 Clark and M. d'Oliveira provided inventory data and derived metrics necessary to run the
476 experiments. A. Ferraz contributed to the data processing. D. Kaki performed a preliminary
477 analysis of the data. V. Meyer prepared the manuscript with contributions from all co-authors.

478

479 The authors declare that they have no conflict of interest.

480

481 **Acknowledgements**

482 The work described in this paper was carried out at the Jet Propulsion Laboratory, California
483 Institute of Technology, under contract with the National Aeronautics and Space Administration.
484 This work has benefited from “*Investissement d’Avenir*” grants managed by the French *Agence*
485 *Nationale de la Recherche* (CEBA, ref. ANR-10-LABX-25-01 and TULIP, ref. ANR-10-LABX-
486 0041; ANAEE-France: ANR-11-INBS-0001) and from CNES (TOSCA project; PI T Le Toan).
487 Field and Lidar data from the Brazilian sites were acquired by the Sustainable Landscapes Brazil
488 project supported by the Brazilian Agricultural Research Corporation (EMBRAPA), the US
489 Forest Service, and USAID, and the US Department of State. La Selva field work was supported
490 by the U.S. National Science Foundation LTREB Program NSF LTREB 1357177. Data in Chocó
491 are available as part of the Reducing Emissions from Deforestation and forest Degradation
492 (REDD) project. FES was supported by Natural Environment Research Council (NERC) grants
493 (‘BIO-RED’ NE/N012542/1 and ‘AFIRE’ NE/P004512/1) and Newton Fund (‘The UK
494 Academies/FAPESP Proc. N°: 2015/50392-8 Fellowship and Research Mobility’). The AGB
495 data for Paracou were made available courtesy of CIRAD (B. Hérault).

496

497 © 2017. All rights reserved.

498

499

500



501 **Data accessibility**

502 The BCI lidar and forest inventory dataset used in this research are publically available from the
503 Office of Bioinformatics, Smithsonian Tropical Research Institute. All relevant data are within
504 the paper and its Supporting Information files.
505

506

507 **References**

508

- 509 Andersen, H. E., Reutebuch, S. E., McGaughey, R. J., d'Oliveira, M. V. and Keller, M.:
510 Monitoring selective logging in western Amazonia with repeat lidar flights. *Remote Sens.*
511 *Environ.*, 151, 157-165, 2014.
512
- 513 Asner, G. P., Mascaro, J., Muller-Landau, H. C., Vieilledent, G., Vaudry, R., Rasamoelina, M.,
514 Hall, J. S. and van Breugel, M.: A universal airborne Lidar approach for tropical forest carbon
515 mapping. *Oecologia*, 168(4), 1147-1160, 2012.
516
- 517 Asner, G. P. and Mascaro, J.: Mapping tropical forest carbon: Calibrating plot estimates to a
518 simple Lidar metric. *Remote Sens. Environ.* 140, 614-624, 2014.
519
- 520 Baker, T. R., Phillips, O. L., Malhi, Y., Almeida, S., Arroyo, L., Di Fiore, A., Erwin, T., Killeen,
521 T. J., Laurance, S. G., Laurance, W. F. and Lewis, S. L.: Variation in wood density determines
522 spatial patterns in Amazonian forest biomass. *Glob. Change Biol.*, 10(5), 545-562. doi:
523 10.1111/j.1365-2486.2004.00751.x, 2004.
524
- 525 Baldocchi, D. D.: Assessing the eddy covariance technique for evaluating carbon dioxide
526 exchange rates of ecosystems: past, present and future. *Glob. Change Biol.*, 9(4), 479-492, 2003.
527
- 528 Basset, Y., Cizek, L., Cuénoud, P., Didham, R. K., Guilhaumon, F., Missa, O., Novotny, V.,
529 Ødegaard, F., Roslin, T., Schmidl, J. and Tishechkin, A. K.: Arthropod diversity in a tropical
530 forest. *Science*, 338(6113), 1481-1484, 2012.
531
- 532 Bastin, J.-F., Barbier, N., Réjou-Méchain, M., Fayolle, A., Gourlet-Fleury, S., Maniatis, D., de
533 Haulleville, T., Baya, F., Beeckman, H., Beina, D. and Couteron, P.: Seeing Central African
534 forests through their largest trees. *Sci. Rep.-UK*, 5, 13156, 2015.
535
- 536 Bioredd.org/ accessed 4.13.2016
537
- 538 Bohlman, S., and O'Brien, S.: Allometry, adult stature and regeneration requirement of 65 tree
539 species on Barro Colorado Island, Panama. *J. Trop. Ecol.*, 22(02), 123-136, 2006.
540



- 541 Brien, R. J. W., Phillips, O. L., Feldpausch T. R., Gloor E., Baker, T. R., Lloyd, J. and Lopez-
542 Gonzalez G.: Long-Term Decline of the Amazon Carbon Sink. *Nature*, 519, 344.
543 <http://dx.doi.org/10.1038/nature14283>, 2015.
544
- 545 Brown, S., Gillespie, A. J., and Lugo, A. E.: Biomass estimation methods for tropical forests
546 with applications to forest inventory data. *Forest Sci.*, 35(4), 881-902, 1989.
547
- 548 Chave, J., Condit, R., Aguilar, S., Hernandez, A., Lao, S., and Perez, R.: Error propagation and
549 scaling for tropical forest biomass estimates, *Philos. T. R. Soc. B*, 359, 409–420, 2004.
550
- 551 Chave, J., Réjou-Méchain, M., Búrquez, A., Chidumayo, E., Colgan, M. S., Delitti, W. B., and
552 Vieilledent, G.: Improved allometric models to estimate the aboveground biomass of tropical
553 trees. *Glob. Change Biol.*, 20(10), 3177-3190, 2014.
554
- 555 Clark D. B. and Clark D. A.: Abundance, growth and mortality of very large trees in neotropical
556 lowland rain forest. *Forest Ecol. and Manag.*, 80, 235–244, 1996.
557
- 558 Clark, D. B. and Clark, D. A.: Landscape-scale variation in forest structure and biomass in a
559 tropical rain forest. *Forest Ecol. and Manag.*, 137, 185–198, 2000.
560
- 561 Condit, R.: *Tropical Forest Census Plots*. Springer Verlag and R.G. Landes Company. Berlin and
562 Georgetown, TX, 1998.
563
- 564 d'Oliveira, M. V. N., Reutebuch, S. E., McGaughey, R. J. and Andersen, H. E. : Estimating
565 forest biomass and identifying low-intensity logging areas using airborne scanning lidar in
566 Antimary State Forest, Acre State, Western Brazilian Amazon. *Remote Sens. Environ.*, 124, 479-
567 491, 2012.
568
- 569 Denslow, J. S. : Gap portioning among tropical rainforest trees. *Biotropica*, 12, 47–55, 1980.
570
- 571 Disney, M. I., Kalogirou, V., Lewis, P., Prieto-Blanco, A., Hancock, S., and Pfeifer, M.:
572 Simulating the impact of discrete-return Lidar system and survey characteristics over young
573 conifer and broadleaf forests. *Remote Sens. Environ.*, 114(7), 1546-1560, 2010.
574
- 575 ENVI/IDL, Exelis Visual Information Solutions, Boulder, Colorado.
576
- 577 Espírito-Santo, F. D. B., Keller, M., Braswell, B., Nelson, B. W., Frohling, S., and Vicente, G.:
578 Storm intensity and old-growth forest disturbances in the Amazon region. *Geophys. Res. Lett.*,
579 37(11), 2010.
580
- 581 Espírito-Santo, F. D. B., Keller, M. M., Linder, E., Oliveira, R. C. Junior, Pereira, C. and
582 Oliveira, C. G.: Gap formation and carbon cycling in the Brazilian Amazon: measurement using
583 high-resolution optical remote sensing and studies in large forest plots. *Plant Ecol. Divers.*, 7,
584 305–318, 2014.
585



- 586 Fauset, S., Johnson, M. O., Gloor, M., Baker, T. R., Monteagudo, A., Brienen, R. J., Feldpausch,
587 T. R., Lopez-Gonzalez, G., Malhi, Y., Ter Steege, H. and Pitman, N. C.: Hyperdominance in
588 Amazonian forest carbon cycling. *Nat. Commun.*, 6, 2015.
589
- 590 Fearnside, P. M.: Wood density for estimating forest biomass in Brazilian Amazonia. *Forest
591 Ecol. and Manag.*, 90(1), 59-87, 1997.
592
- 593 Ferraz, A., Saatchi, S., Mallet, C., and Meyer, V.: Lidar detection of individual tree size in
594 tropical forests. *Remote Sens. Environ.*, 183, 318-333, 2016.
595
- 596 Figueiredo, E. O., d'Oliveira, M. V. N., Braz, E. M., de Almeida Papa, D. and Fearnside, P. M.:
597 LIDAR-based estimation of bole biomass for precision management of an Amazonian forest:
598 Comparisons of ground-based and remotely sensed estimates. *Remote Sens. Environ.*, 187, 281-
599 293, 2016.
600
- 601 Gentry, A. H.: Four neotropical rainforests. Yale University Press, 1993.
602
- 603 Goldstein, G., Andrade, J. L., Meinzer, F. C., Holbrook, N. M., Cavellier, J., Jackson, P., and
604 Celis, A.: Stem water storage and diurnal patterns of water use in tropical forest canopy trees.
605 *Plant Cell Environ.*, 21(4), 397-406, 1998.
606
- 607 Goodman, R. C., Phillips, O. L., and Baker, T. R.: The importance of crown dimensions to
608 improve tropical tree biomass estimates. *Ecol. Appl.*, 24(4), 680-698, 2014.
609
- 610 Gourlet-Fleury, S., Guehl, J.-M. and Laroussinie, O.: Ecology and management of a neotropical
611 rainforest. Lessons drawn from Paracou, a long-term experimental research site in French
612 Guiana. Elsevier, Amsterdam, 2004.
- 613 Hirata, Y.: The effects of footprint size and sampling density in airborne laser scanning to extract
614 individual trees in mountainous terrain. *Proc. ISPRS WG VIII/2 "Laser-scanners for forestry and
615 landscape assessment"*, Vol. XXXVI, Part 8/W2, 3-6 October 2004, Freiburg, Germany, 2004.
- 616 Hopkinson, C.: The influence of flying altitude, beam divergence, and pulse repetition frequency
617 on laser pulse return intensity and canopy frequency distribution. *Can. J. Remote Sens.*, 33(4),
618 312-324, 2007.
619
- 620 Hubbell, S. P., Foster, R. B., O'Brien, S. T., Harms, K. E., Condit, R., Wechsler, B., Wright, S. J.
621 and De Lao, S. L.: Light gap disturbances, recruitment limitation, and tree diversity in a
622 neotropical forest. *Science*, 283, 554-557, 1999.
623
- 624 Jubanski, J., Ballhorn, U., Kronseder, K., Franke, J., and Siegert, F.: Detection of large above-
625 ground biomass variability in lowland forest ecosystems by airborne Lidar. *Biogeosciences*,
626 10(6), 3917-3930, 2013.
627
- 628 Kellner, J. R., and Asner, G. P.: Convergent structural responses of tropical forests to diverse
629 disturbance regimes. *Ecol. Lett.*, 12(9), 887-897, 2009.



- 630
631 Laurance, W. F., Delamônica, P., Laurance, S. G., Vasconcelos, H. L., and Lovejoy, T. E.:
632 Conservation: rainforest fragmentation kills big trees. *Nature*, 404(6780), 836-836.
633 doi:10.1038/35009032, 2000.
634
635 Le Toan, T., Quegan, S., Davidson, M. W. J., Balzter, H., Paillou, P., Papathanassiou, K.,
636 Plummer, S., Rocca, F., Saatchi, S., Shugart, H. and Ulander, L.: The BIOMASS mission:
637 Mapping global forest biomass to better understand the terrestrial carbon cycle. *Remote Sens.*
638 *Environ.*, 115(11), 2850-2860, 2011.
639
640 Lefsky, M. A., Cohen, W. B., Parker, G. G., and Harding, D. J.: Lidar remote sensing for
641 ecosystem studies, *BioScience*, 52, 19–30, 2002.
642
643 Lefsky, M. A.: A global forest canopy height map from the Moderate Resolution Imaging
644 Spectroradiometer and the Geoscience Laser Altimeter System. *Geophys. Res. Lett.*, 37(15),
645 2010.
646
647 Lefsky, M. A., Keller, M., Pang, Y., De Camargo, P. B., and Hunter, M. O.: Revised method for
648 forest canopy height estimation from Geoscience Laser Altimeter System waveforms. *J. Appl.*
649 *Remote Sens.*, 1(1), 013537, 2007.
650
651 Leitold, V., Keller, M., Morton, D. C., Cook, B. D., and Shimabukuro, Y. E.: Airborne Lidar-
652 based estimates of tropical forest structure in complex terrain: opportunities and trade-offs for
653 REDD+. *Carbon Balance Management*, 10(1), 3, 2015.
654
655 Mascaro, J., Detto, M., Asner, G. P., and Muller-Landau, H. C.: Evaluating uncertainty in
656 mapping forest carbon with airborne Lidar. *Remote Sens. Environ.*, 115, 3770-3774, 2011.
657
658 Meyer, V., Saatchi, S. S., Chave, J., Dalling, J. W., Bohlman, S., Fricker, G. A., Robinson, C.,
659 Neumann, M., and Hubbell, S.: Detecting tropical forest biomass dynamics from repeated
660 airborne Lidar measurements. *Biogeosciences*, 10(8), 5421-5438, 2013.
661
662 Minh, D. H. T., Le Toan, T., Rocca, F., Tebaldini, S., Villard, L., Réjou-Méchain, M., Phillips,
663 O. L., Feldpausch, T.R., Dubois-Fernandez, P., Scipal, K. and Chave, J.: SAR tomography for
664 the retrieval of forest biomass and height: Cross-validation at two tropical forest sites in French
665 Guiana. *Remote Sens. Environ.*, 175, 138-147, 2016.
666
667 Nepstad, D. C., Tohver, I. M., Ray D., Moutinho, P., and Cardinot, G.: Mortality of large trees
668 and lianas following experimental drought in an Amazon forest. *Ecology* 88, 2259–2269, 2007.
669
670 Nogueira, E. M., Fearnside, P. M., Nelson, B. W., and França, M. B.: Wood density in forests of
671 Brazil's 'arc of deforestation': Implications for biomass and flux of carbon from land-use change
672 in Amazonia. *Forest Ecol. and Manag.*, 248(3), 119-135, 2007.
673



- 674 Packalen, P., Strunk, J. L., Pitkänen, J. A., Temesgen, H., and Maltamo, M.: Edge-tree correction
675 for predicting forest inventory attributes using area-based approach with airborne laser scanning.
676 IEEE J. Sel. Top. Appl., 8(3), 1274-1280, 2015.
677
- 678 Pascual, M., and Guichard, F.: Criticality and disturbance in spatial ecological systems. Trends
679 Ecol. Evol., 20(2), 88-95, 2005.
680
- 681 Pearson, T. R., Brown, S., and Casarim, F. M.: Carbon emissions from tropical forest
682 degradation caused by logging. Environ. Res. Lett., 9(3), 034017, 2014.
683
- 684 Phillips, O. L., Malhi, Y., Higuchi, N., Laurance, W. F., Núñez, P. V., Vásquez, R. M.,
685 Laurance, S. G., Ferreira, L. V., Stern, M., Brown, S. and Grace, J.: Changes in the carbon
686 balance of tropical forests: evidence from long-term plots. Science, 282(5388), 439-442, 1998.
687
- 688 Phillips, O. L., Aragão, L. E., Lewis, S. L., Fisher, J. B., Lloyd, J., López-González, G., Malhi,
689 Y., Monteagudo, A., Peacock, J., Quesada, C. A. and Van Der Heijden, G.: Drought sensitivity
690 of the Amazon rainforest. Science, 323(5919), 1344-1347, 2009.
691
- 692 Popescu, S. C., Wynne, R. H., and Nelson, R. F.: Measuring individual tree crown diameter with
693 Lidar and assessing its influence on estimating forest volume and biomass. Can. J. Remote Sens.,
694 29(5), 564-577, 2003.
695
- 696 R Core Team, 2014. R: A language and environment for statistical computing. R Foundation for
697 Statistical Computing, Vienna, Austria. URL <http://www.R-project.org/>.
698
- 699 Réjou-Méchain, M., Tymen, B., Blanc, L., Fauset, S., Feldpausch, T. R., Monteagudo, A.,
700 Phillips, O. L., Richard, H. and Chave, J.: Using repeated small-footprint Lidar acquisitions to
701 infer spatial and temporal variations of a high-biomass Neotropical forest. Remote Sens.
702 Environ., 169, 93-101, 2015.
703
- 704 Rocca, F., Dinh, H. T. M., Le Toan, T., Villard, L., Tebaldini, S., d'Alessandro, M. M., and
705 Scipal, K.: Biomass tomography: A new opportunity to observe the earth forests. Int. Geosci.
706 Remote Se., 1421-1424, 2014.
707
- 708 Saatchi, S. S., Harris, N. L., Brown, S., Lefsky, M., Mitchard, E.T., Salas, W., Zutta, B. R.,
709 Buermann, W., Lewis, S. L., Hagen, S. and Petrova, S.: Benchmark map of forest carbon stocks
710 in tropical regions across three continents. P. Natl Acad. Sci. USA, 108(24), 9899-9904, 2011.
711
- 712 Saatchi, S. S., Asefi-Najafabady, S., Malhi, Y., Aragão, L. E., Anderson, L. O., Myneni, R. B.,
713 and Nemani, R.: Persistent effects of a severe drought on Amazonian forest canopy. P. Natl
714 Acad. Sci. USA, 110(2), 565-570, 2013.
715
- 716 Santiago, L. S., Goldstein, G., Meinzer, F. C., Fisher, J. B., Machado, K., Woodruff, D., and
717 Jones, T.: Leaf photosynthetic traits scale with hydraulic conductivity and wood density in
718 Panamanian forest canopy trees. Oecologia, 140(4), 543-550, 2004.
719



- 720 Simard, M., Pinto, N., Fisher, J. B., and Baccini, A.: Mapping forest canopy height globally with
721 spaceborne lidar, *Journal of Geophysical Research - Biogeosciences*, 116, G04021,
722 doi:10.1029/2011JG001708, 2011.
723
- 724 Slik, J. W., Paoli, G., McGuire, K., Amaral, I., Barroso, J., Bastian, M., Blanc, L., Bongers, F.,
725 Boundja, P., Clark, C. and Collins, M. : Large trees drive forest aboveground biomass variation
726 in moist lowland forests across the tropics. *Global Ecol. and Biogeogr.*, 22(12), 1261-1271,
727 2013.
728
- 729 Solé, R. V., and Manrubia, S. C.: Are rainforests self-organized in a critical state?. *J. Theor.*
730 *Biol.*, 173(1), 31-40, 1995.
731
- 732 Strigul, N., Pristinski, D., Purves, D., Dushoff, J., and Pacala, S.: Scaling from trees to forests:
733 tractable macroscopic equations for forest dynamics. *Ecol. Monogr.*, 78(4), 523-545, 2008.
734
- 735 Ter Steege, H., Pitman, N. C., Phillips, O. L., Chave, J., Sabatier, D., Duque, A., Molino, J. F.,
736 Prévost, M. F., Spichiger, R., Castellanos, H. and Von Hildebrand, P.: Continental-scale patterns
737 of canopy tree composition and function across Amazonia. *Nature*, 443(7110), 444-447, 2006.
738
- 739 Ter Steege, H., Pitman, N.C., Sabatier, D., Baraloto, C., Salomão, R. P., Guevara, J.E., Phillips,
740 O. L., Castilho, C. V., Magnusson, W. E., Molino, J. F. and Monteagudo, A. :Hyperdominance
741 in the Amazonian tree flora. *Science*, 342(6156), 1243092, 2013.
742
- 743 Vauhkonen, J., Ene, L., Gupta, S., Heinzl, J., Holmgren, J., Pitkänen, J., Solberg, S., Wang, Y.,
744 Weinacker, H., Hauglin, K. M. and Lien, V.: Comparative testing of single-tree detection
745 algorithms under different types of forest. *Forestry*, 85(1), 27-40, 2011.
746
- 747 Vauhkonen, J., Næsset, E., and Gobakken, T.: Deriving airborne laser scanning based
748 computational canopy volume for forest biomass and allometry studies. *ISPRS J. Photogramm.*,
749 96, 57-66, 2014.
750
- 751 Vincent, G., Sabatier, D., Blanc, L., Chave, J., Weissenbacher, E., Péliissier, R., Fonty, E.,
752 Molino, J. F. and Coueron, P.: Accuracy of small footprint airborne Lidar in its predictions of
753 tropical moist forest stand structure. *Remote Sens. Environ.*, 125, 23-33, 2012.
754
- 755 West, G.B., Enquist, B. J. and Brown, J. H. : A general quantitative theory of forest structure and
756 dynamics. *P. Natl Acad. Sci. USA*, 106, 7040–7045, 2009.
757
- 758 Zhou, J., Proisy, C., Descombes, X., Hedhli, I., Barbier, N., Zerubia, J., Gastellu-Etchegorry, J.
759 P. and Coueron, P.: Tree crown detection in high resolution optical and Lidar images of tropical
760 forest. *P. Soc. Photo-Opt. Ins.*, 7824. SPIE, 2010.
761 , 2010.
762

763



764
765
766
767
768
769
770
771

Table 1. Information on forest inventory plots. * indicates that a site has been used for the calibration of the LCA model. Sources: Antimary and Cotriguaçu: Fearnside, 1997; d'Oliveira et al., 2012, BCI: Center for Tropical Forest Science (CTFS) (Condit, 1998; Hubbell et al., 1999, 2005), Chocó: (bioredd.org), La Selva: Carbono project (Clark and Clark, 2000), Manaus and Tapajós: Espírito-Santo (unpublished results), Nouragues: Réjou-Méchain et al., 2015, Paracou: Gourlet-Fleury et al., 2004; Vincent et al., 2012.

Site	Data	Plots Size (ha)	N plots	Year	Mean WD (g cm ⁻³)	Mean AGB (Mg ha ⁻¹)	Annual rainfall (mm yr ⁻¹)
Antimary (Brazil)	Plot level	0.25	50	2010	0.61	234	2000
BCI * (Panama)	Tree level	1	50	2010	0.56	235	2600
Chocó (Colombia)	Tree level	0.25	42	2013	0.60	224	10000
Cotriguaçu (Brazil)	Not available	-	-	-	0.60	-	2000
La Selva * (Costa Rica)	Tree level	1	11	2009	0.45	178	4000
Manaus (Brazil)	Tree level	0.25	10	2014	0.66	263	2200
Nouragues * (French Guiana)	Plot level Tree level	1 1	33 7/33	2012	0.66	424	3000
Paracou * (French Guiana)	Plot level	1	85	2009-10	0.71	353	3000
Tapajós (Brazil)	Tree level	0.25	10	2014	0.62	238	1900

772
773



774 **Table 2.** Information on Lidar data and locations of the 9 research sites.

Site	Sensor	Year	Retur	Flight	Scanning	Frequency	NW corner lat	NW corner lon
(1km ² images)			ns m ²	Altitude (m)	angle (°)	(kHz)		
Antimary	Optech ALTM3100EA	2010-2011	10-15	500	11	70	9°17'47.26"S	68°17'15.06"W
BCI	Optech ALTM3100EA	2009	8	1000	35	70	9°9'28.56"N	79°51'18.9"W
Chocó	Optech ALTM3033	2013	4	1000	20	33	3°57'5.71"N	76°49'10.31"W
Cotriguaçu	Optech ALTM3100EA	2011	10-15	850	11	60	9°27'8.87"S	58°51'51.22"W
La Selva	Optech ALTM3100EA	2009	4	1500	20	70	10°25'37.97"N	84°1'8.76"W
Manaus	Optech ALTM3100EA	2012	10-15	850 (max)	11	60	2°56'38.48"S	59°56'12.57"W
Nouragues	Riegl LMS-Q560	2012	12	400	45	200	4°3'10.0"N	52°42'19.95"W
Paracou	Riegl LMS-280i	2009	4	120-220	30	24	5°15'47.73"N	52°56'26.96"W
Tapajós	Optech ALTM3100EA	2011	10-15	850 (max)	11	60	2°50'53.41"S	54°57'44.53"W

775

776



777 **Table 3.** Coefficients, R^2 , RMSE and bias for the models used to estimate AGB_{LCA} without and with wood density
778 as a weighting factor (m_LCA) and m_LCA_wd, respectively).

Model	Equation	a	b	R^2	RMSE	Bias	R^2 cross-val	RMSE cross-val	Bias cross-val
m_LCA	$AGB = aLCA + b$ (Eq. (2))	3.56	136.91	0.59	62.53	0.0	0.58	63.26	0.16
m_LCA_wd	$AGB = (aLCA+b) \times WD$ (Eq. (3))	4.47	270.27	0.78	46.02	-0.76	0.77	46.47	-0.63

779

780



781

782 **Figure 1.** Segmentation of the 1 km × 1 km images in each site using five canopy height thresholds. A minimum of
783 100 contiguous pixels was used as a segmentation threshold in all cases.

784 **Figure 2 :** LCA in function of height thresholds in the nine study sites. The steepest slopes are between 24 m
785 (Antimary) and 30 m (Nouragues), with an average of 27 m across sites. Steepness of slope was obtained by
786 calculating the derivative of the sigmoid models characterizing each site.
787

788 **Figure 3.** Distribution of R^2 between tree height thresholds used to determine LCA and AGB_{Lidar} in the nine 1 ha
789 subareas (a) and distribution of R^2 between tree height thresholds and AGB_{inv} in 1 ha inventory plots of the four
790 calibration sites (b). All optimal thresholds are between 23 m and 30 m. The average maximal height threshold is 27
791 m.
792

793 **Figure 4.** Relationship between AGB_{inv} density and LCA (a) and AGB density normalized by averaged wood (b).
794 Normalizing AGB by averaged wood density brings the data from different sites closer to a common fit.
795

796 **Figure 5.** AGB_{inv} density vs. AGB_{LCA} estimated with LCA_wd model (a). AGB_{Lidar} density from the 1km² images
797 vs. AGB_{LCA} estimated with LCA_wd model (b). The black line represents the 1-to-1 line.
798

799 **Figure 6.** Detection of changes of forest structure from selective logging in the Antimary study area showing a) the
800 difference between pre- and post- logging (2010–2011) Lidar derived LCA at 1 ha grid cells over the entire study
801 area, b) the histogram of LCA for the two Lidar datasets showing the mean difference and the reduction of medium
802 and large LCA areas from selective logging, c) 2010 Lidar LCA segmentation at 1 m resolution over a sample area
803 in the north of the study site, d) same LCA segmentation for 2011 Lidar data, and e) difference of the two segmented
804 areas showing the extent of the logging impact on large trees in addition to natural changes of forest structure from
805 changes in canopy gaps from tree falls and tree growth.
806

807 **Figure 7.** Relationship between LCA and AGB_{LCA} (a) and relationship between AGB_{inv} of large trees (>50 cm
808 DBH) and total AGB_{inv} (b). In both cases, the intercepts represent the contribution of small trees to total AGB. Note
809 that Manaus and Nouragues overlap because they have the same mean wood density, as well as Chocó and
810 Cotriguaçu.
811

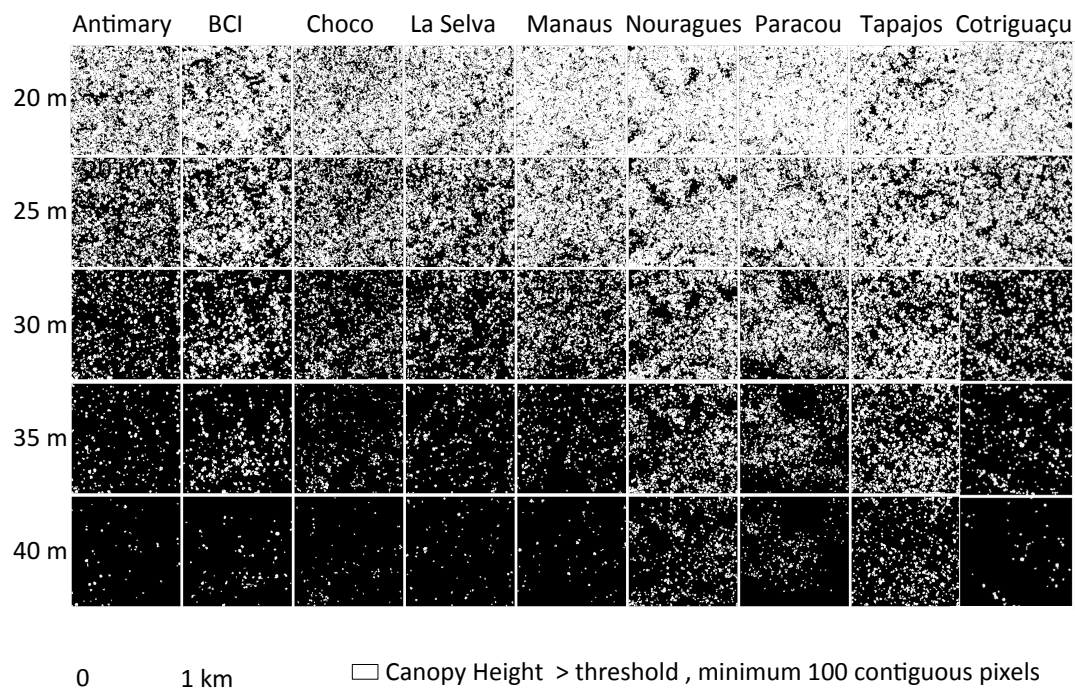
812

813

814



815 Figure 1

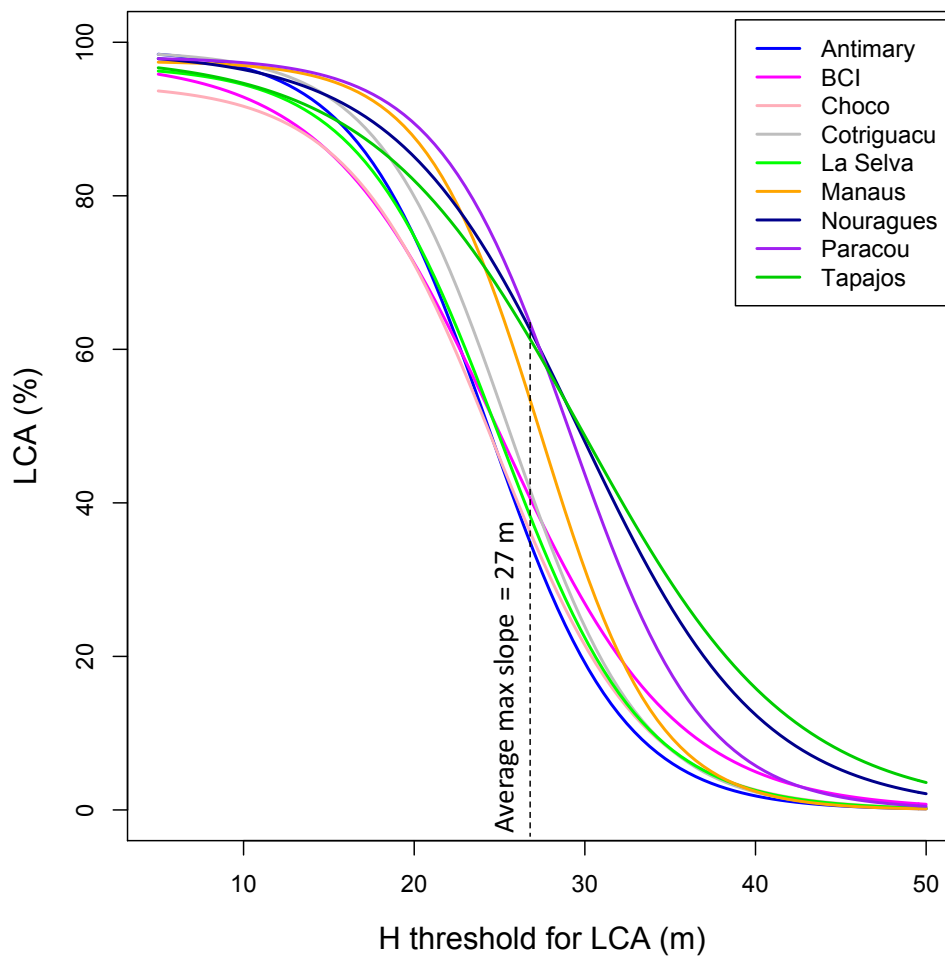


816

817



818 Figure 2

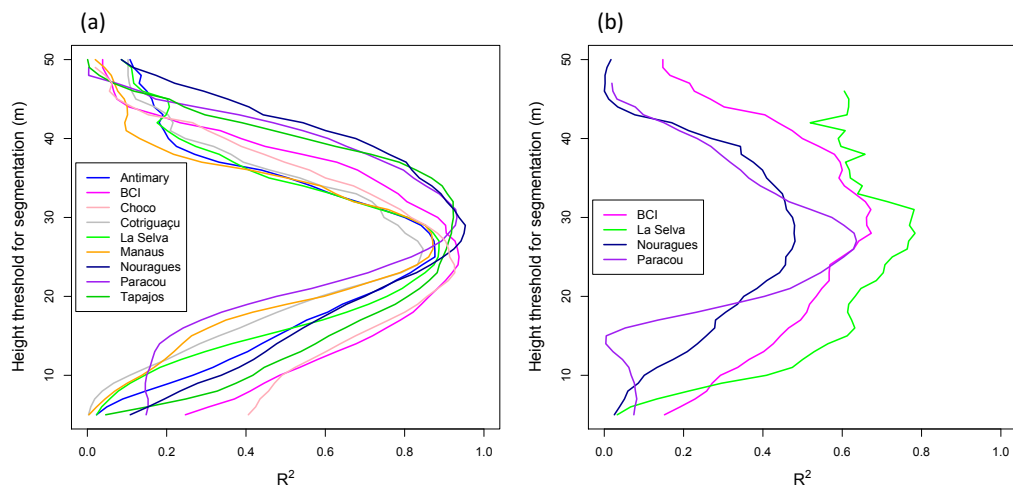


819

820



821 Figure 3

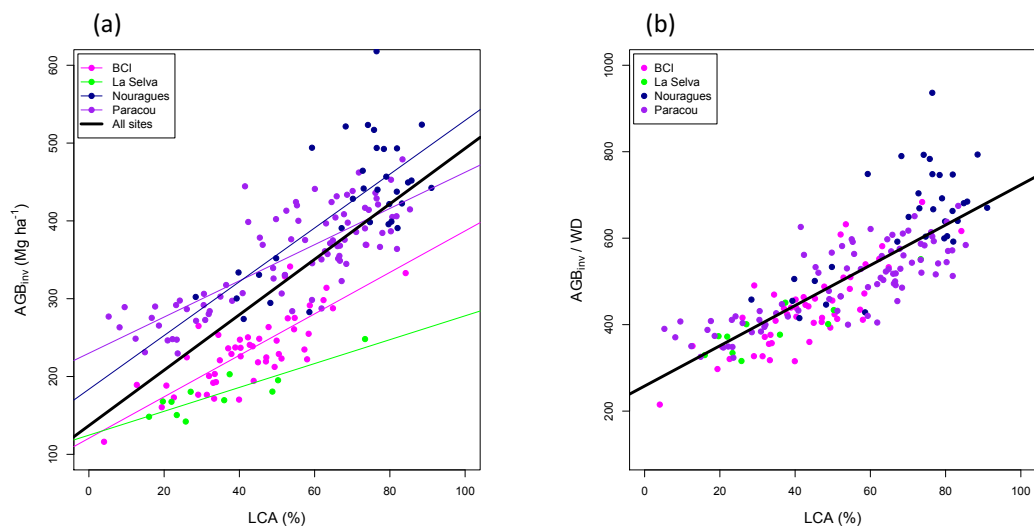


822

823



824 Figure 4

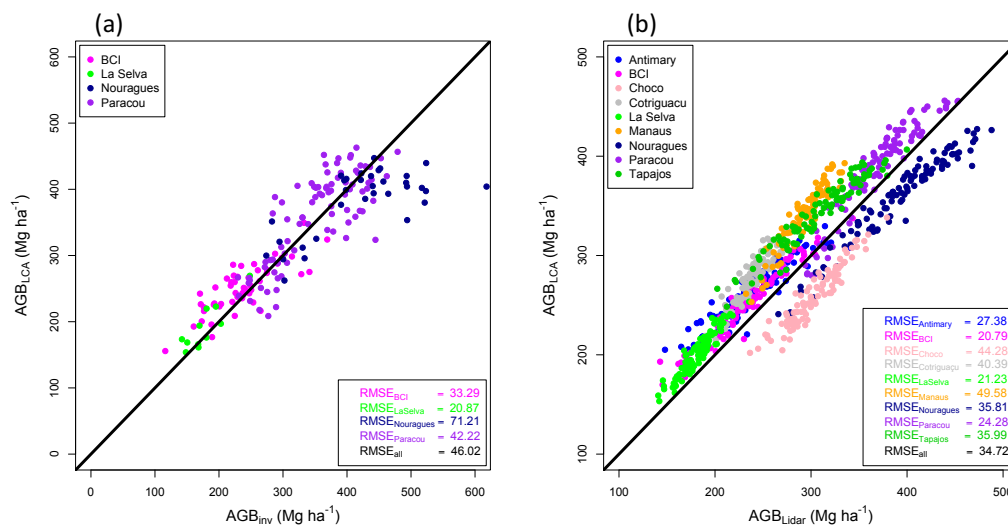


825

826



827 Figure 5



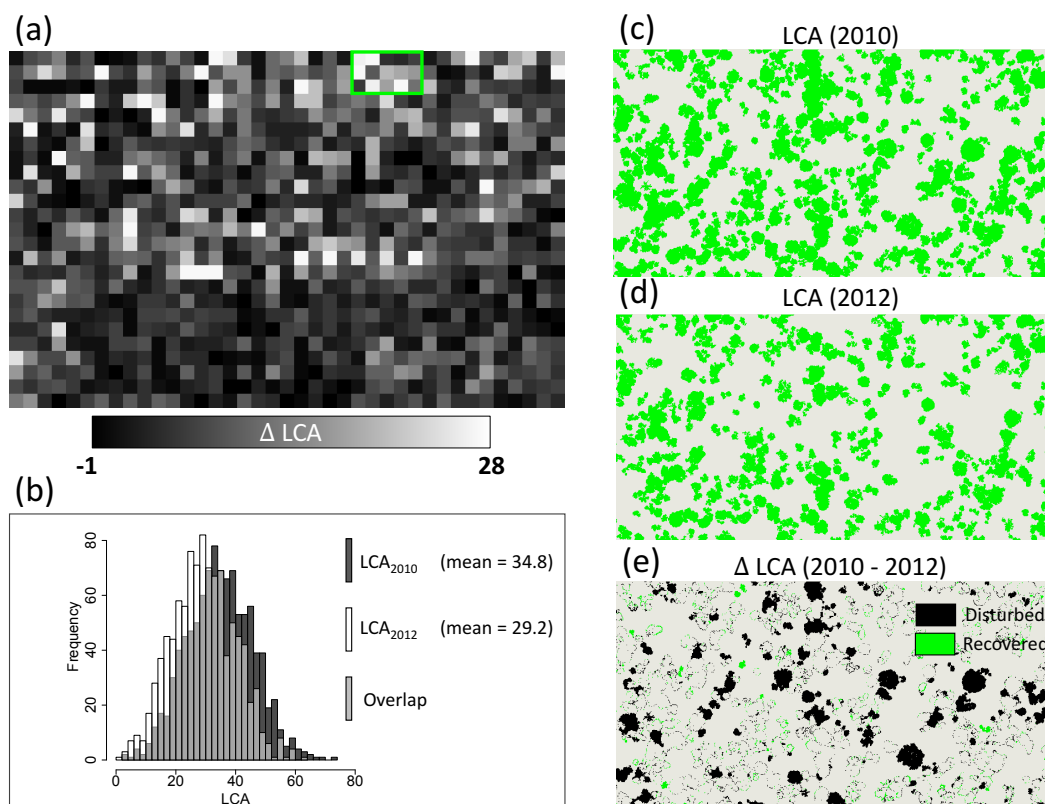
828

829

830



831 Figure 6

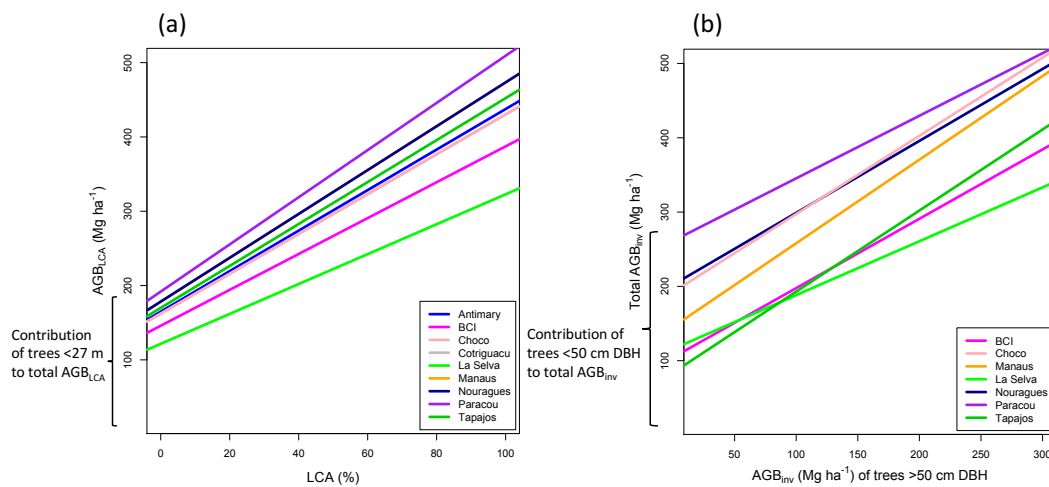


832

833



834 Figure 7



835